PHYSICAL REVIEW E **75**, 056113 (2007)

Self-assembly of flat sheets into closed surfaces

Silas Alben* and Michael P. Brenner
Division of Engineering and Applied Sciences, Harvard University, Cambridge, Massachusetts 02138, USA

(Received 6 February 2007; published 23 May 2007)

A recent experiment [Boncheva *et al.* Proc. Natl. Acad. Sci. U.S.A. **102**, 3924 (2005)] introduced the possibility of initiating the self-assembly of a three-dimensional structure from a flat elastic sheet. The ultimate utility of this method for assembly depends on whether it leads to incorrect, metastable structures. Here we examine how the number of metastable states depends on the sheet shape and thickness. Using simulations and theory, we identify out-of-plane buckling as the key event leading to metastability. The buckling strain that arises from joining edges of a planar sheet can be estimated using the theory of dislocations in elastic media. The number of metastable states increases rapidly with increasing variability in the boundary curvature and decreasing sheet thickness.

DOI: 10.1103/PhysRevE.75.056113 PACS number(s): 81.16.Dn, 46.32.+x, 46.70.De

INTRODUCTION

Methods for self-assembly have traditionally focused on bringing together identical building blocks into a desired configuration. The most natural strategy is to design an energy landscape with the desired outcome as the energy minimum [2,3]. The primary difficulty with this strategy is the prevalence of local minima. For example, if we consider clusters of N particles interacting through a van der Waals potential, the number of local minima increases from at least 4 for $N=7$ to 988 for $N=13$ [4]. For this reason successful assembly strategies have generally employed patterned surfaces or templates to decrease the number of local minima [5–10].

Recently Boncheva *et al.* have outlined a completely different paradigm for self-assembly [1]. Instead of basing the self-assembly on small building blocks, they consider the spontaneous folding of a planar elastic sheet into a (prespecified) closed surface, driven by interacting elements on the surface of the sheet. Three different sheet shapes were chosen (see Fig. 1), all of which can be naturally assembled into a sphere. These sheets were fabricated out of the elastomer polydimethylsiloxane, with small rigid magnets as interacting elements. Whether the sheet folded into a sphere depended critically on (i) the shape of the sheet, (ii) the locations of the interacting elements, and (iii) the nature of the external forcing that was applied during the assembly. For example, the shape in Fig. 1(a) required the action of capillary forces and gravity to fold correctly. The shape misfolded when suspended in water. The shape in Fig. 1(f) folded only when shaken vigorously, while that in Fig. 1(j) required only mild agitation to facilitate folding. The fact that some of the sheets misfold illustrates that this system can be plagued with multiple equilibria. The potential for misfolding depends on the design choices for the shape of the sheet and the locations of the interacting elements.

The experimental design strategy was to place magnetic loops on the closed sheet, then cut open and flatten the sheet and attached magnets into the plane. The idea behind this strategy was that once the structure was released from its support, the magnets would minimize energy by reforming the loops, and thus close the sheet. In general, this is a global strategy, because the folding depends on the attraction between magnets at the ends of the open loops, which may be at a distance as large as the sheet size. In our simulations we find that two of the three successful structures actually succeed because the closest attracting elements connect first. Consequently, the edges are gradually brought together in a series of local attractions. We term this process "zipping."

The goal of this paper is to understand how the choices of sheet shape and thickness influence the success of self-assembly through zipping. Using theory and numerical simulations, we find that the primary mechanism for assembly of an elastic sheet is buckling due to the induced strain from bringing edges together. We demonstrate that buckling is also the essential feature leading to metastability, since each buckling event can result in two possible final configurations for every pair of edges that are brought together. Hence the number of metastable states can increase exponentially with the number of edge pairs. Our simulations demonstrate that in practice there is mechanical coupling between nearby edge pairs, which decreases the number of attainable configurations.

I. NUMERICAL MODEL OF FLAT SHEETS WITH ATTRACTING ELEMENTS

We have numerically simulated the three sheet shapes studied in the experiment, with distributions of attracting elements on their edges. We discretize the sheet using an equilateral-triangular lattice of springs, following the method of Seung and Nelson [11]. The lattice is obtained by superposing a parametrization of the experiment's two-dimensional (2D) boundary curve on a uniform hexagonal lattice (see Fig. 1), and selecting those faces with centroids contained within the boundary curve. The set of faces and their included edges and vertices comprises the discrete representation of the sheet.

The stretching energy for the sheet is given by the stretching of springs between neighboring vertices, and the bending energy is given by the angle between adjacent triangular

---

*Electronic address: alben@deas.harvard.edu

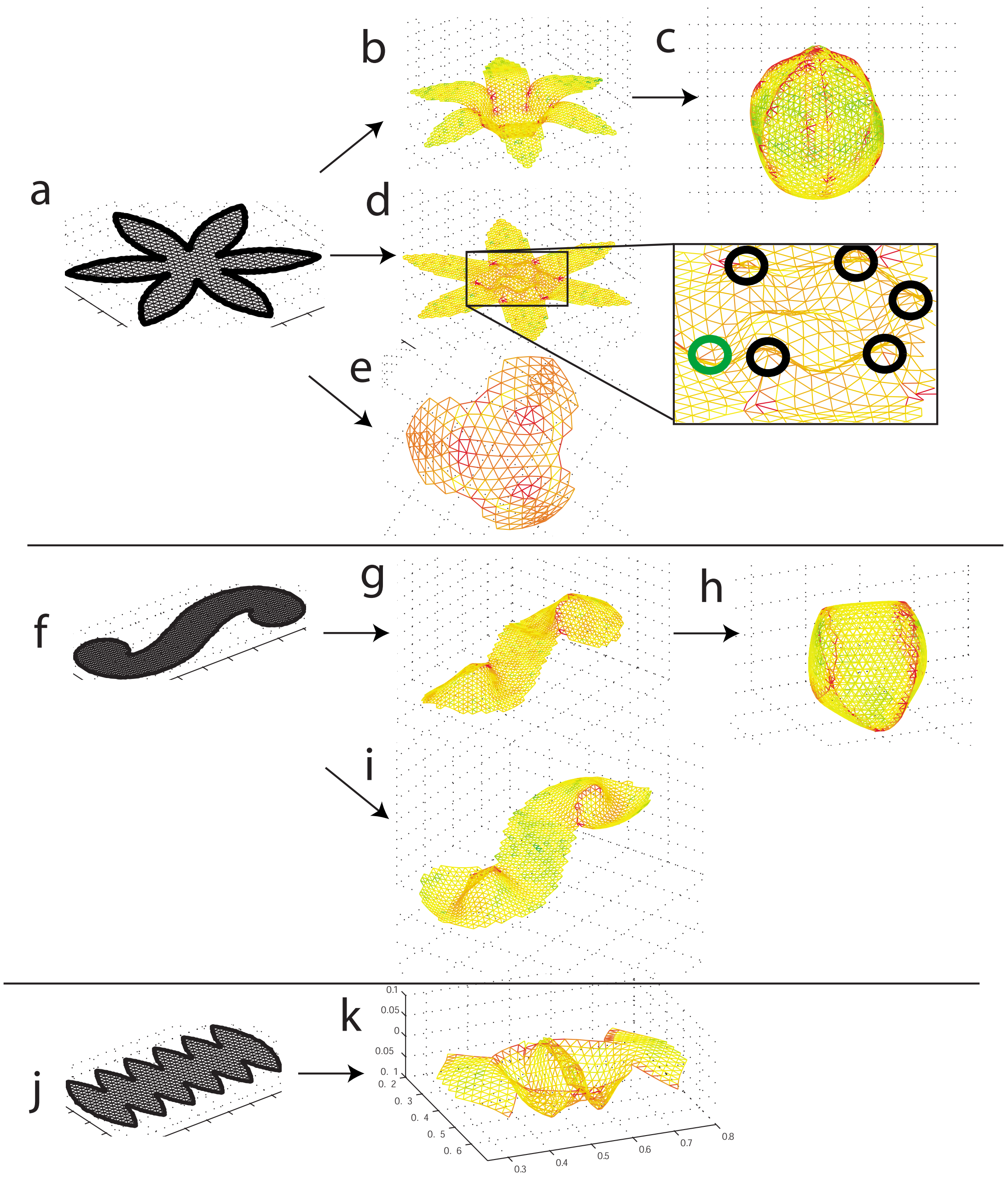

FIG. 1. (Color online) Representative cases for the assembly of flat sheets into curved surfaces. (a) Discretization of the shape used by Boncheva *et al.* for the “flower” cut. (b) A case where the random initial condition [out-of-plane displacements of $O(10^{-10})$] leads to the same sign of curvature at all cusps of the flower cut after buckling. The ratio of stretching to bending energy is $\gamma=10^5$ [see Eq. (2)]. The magnitude of stretching strain is visualized by intensity. Light gray (or green) corresponds to low values of strain and dark gray (or red) to high values. (c) The assembled flower cut. (d) An initial buckling of the flower cut when five of the six cusps buckle upward (inset, black circles), and one buckles downward [inset, gray (green) circle]. Such wrong-signed initial curvature persists in the final state of the sphere. (e) Simulation of the final equilibrium of the flower shape with alternating positive and negative charges at the tips [with a discretization which is coarser than that in (a)–(d)]; misfolding occurs due to an instability among multiple interacting charges. (f) Discretization of the shape used by Boncheva *et al.* for the “orange peel” cut. (g) An intermediate stage in the assembly of the orange peel cut, in which the initial buckling has the same sign at both cusps. Here $\gamma=10^4$. (h) The final assembled orange peel cut, showing a concentration of stretching strain near the boundary. The stretching strain decays rapidly from a maximum of 20% at the boundary to less than 2% within 90% of the sheet. (i) A simulation of the orange peel shape, where the charges are sufficiently strong to join the edges before the shape equilibrates elastically from previous zipping steps. The zipping deviates sufficiently from the case in (g) that incorrect curvature occurs. (j) Discretization of the shape used by Boncheva *et al.* for the “equator cut.” (k) A simulation of the equator cut shape during zipping, showing an example of the generic phenomenon in which neighboring cusps have opposite-signed curvature, thus preventing the successful zipping of the equator cut into a sphere. Here $\gamma=2.5\times10^4$.

faces. The electrostatic energy is a sum over pairwise Coulomb forces at the sheet vertices. The total energy is thus

$$U = \frac{\sqrt{3}Y}{4}\sum_{i,j}(r_{ij}-r_{ij}^{eq})^2 + \tilde{\kappa}\sum_{\alpha,\beta}(1-\mathbf{n}_\alpha\cdot\mathbf{n}_\beta) + \sum_{k,l} k_c\frac{q_k q_l}{r_{kl}}\eta_\epsilon(r_{kl}), \tag{1}$$

where Y is the 2D Young's modulus, r_{ij} is the distance between neighboring vertices with equilibrium distance r_{ij}^{eq}, $\tilde{\kappa}$ is the sheet bending rigidity, and $\mathbf{n}_\alpha$ and $\mathbf{n}_\beta$ are normals to neighboring faces. The first two terms on the right side of Eq. (1) tend to the energies of an isotropic elastic sheet with 2D Young's modulus Y, bending rigidity $\tilde{\kappa}$, and Poisson ratio $\nu=1/3$ in the continuum limit (i.e., when the ratio of the bond length r_{ij}^{eq} to sheet size R goes to zero) [11]. The bending rigidity may be expressed in terms of Y, ν, and the sheet thickness h as $\tilde{\kappa}=Yh^2/12(1-\nu^2)$. In the Coulombic term, q_k and q_l are strengths of point charges fixed to the sheet and separated by a distance r_{kl}, and η_ϵ cuts off the $1/r$ singularity within a distance of order ϵ (if ϵ is sufficiently small it does not affect the dynamics—see Appendix A). Charges are distributed over the edges of the sheet. We are thus able to model all of the magnetic configurations in the experiment, since assembly is driven by the interaction of elements on the sheet edges.

The main advantage of the triangulated-mesh method for simulating elastic sheets is its simplicity and computational speed. Previous workers have used triangulated-mesh models to simulate elastic sheets in problems of quasistatic crumpling, with prescribed forcing at the boundaries [12].

We simulate assembly using two different dynamical rules. The first rule assumes overdamped dynamics, in which the velocity of each vertex on the sheet is proportional to the force on it [equal to the gradient of the energy in Eq. (1)]; the second rule assumes a quasistatic approximation to overdamped dynamics. Here the edges of the sheet are joined in a series of small discrete increments. When each increment is joined, the rest of the sheet is assumed to relax to elastic equilibrium. To complete the specification of quasistatic dynamics, one must specify the order in which the different points on the edges are to connect. Note that the r^{-2} decay of Coulomb forces causes a strong bias in favor of nearby charge pairs, whose attraction is only weakly affected by distant charges. A natural order for assembly of points along a given pair of edges therefore consists of connecting lattice points in order of proximity, beginning at the point where the edges meet. Finally, we specify the order in which pairs of points on different edges connect according to the charge distributions being simulated. Different orderings can lead to different elastic energy minima accessible through quasistatic dynamics. The advantage of the quasistatic dynamics is that it is faster to simulate than overdamped dynamics.

A simulation of quasistatic dynamics requires a discrete energy minimization when each pair of charges is joined. In our quasistatic simulations, we evolve the sheet through a large number of elastic equilibria, at each stage performing an energy minimization in a high-dimensional space. We use a standard quasi-Newton method known as limited-memory Broyden-Fletcher-Goldfarb-Shanno (LM-BFGS), a limited-memory Broyden method [16]. This method is efficient for energy minimization and requires moderate computer time to converge to a minimum-energy state. For our typical mesh size there are $O(10^3)$ degrees of freedom, and $O(10^3)$ evaluations of the energy gradient are needed. Our simulation of overdamped dynamics uses second-order Runge-Kutta time stepping. Small time steps are required to simulate the motion of charges accurately, which makes the dynamics more computationally expensive than quasistatic dynamics.

II. RESULTS AND DISCUSSION

We have simulated the assembly of the three sheets studied in the experiment of Boncheva *et al.*, and representative examples are shown in Fig. 1. The discretized flower-petal sheet in Fig. 1(a) is simulated quasistatically by joining points moving outward from each cusp along the six edge pairs. The six edge pairs are joined simultaneously. When enough points have been joined, the sheet becomes unstable to out-of-plane motion. Under a small initial out-of-plane displacement, the sheet may buckle into the configuration shown in Fig. 1(b). Subsequent joining of edges leads finally to the approximate sphere shown in Fig. 1(c). Large stretching strain is concentrated along edges of the sheet throughout the dynamics. For a different initial out-of-plane perturbation, we obtain the state in Fig. 1(d). Here five cusps buckle with the same sign of curvature and one with opposite sign. This structure does not subsequently fold into a closed shape. Simulations using overdamped dynamics have given the same sheet configurations. In Fig. 1(e), we show the result of a simulation of the flower-petal sheet using an alternative configuration of attracting elements introduced by Boncheva *et al.* Here we place alternating positive and negative charges only at each of the six tips of the petals, and not along the edges. We use overdamped dynamics with a mesh which is coarser than that in Figs. 1(a)–1(d). After buckling out of plane as in Fig. 1(b), the six tips approach the center of the sheet radially. However, at a certain distance the tips become unstable to a pairing-up motion. Finally, as shown in Fig. 1(e), the sheet reaches an undesired equilibrium with the six petals joined into three pairs in a nonclosed shape.

Simulations of the orange peel cut, shown in Figs. 1(f)–1(h), show a sequence of states similar to that for the successful flower petal when assembly is successful here also: the sheet becomes unstable to out-of-plane buckling at the (two) cusps, which leads to the final shape in Fig. 1(h) when both buckle with the same sign of curvature; if not, the final state is a nonclosed shape (not shown). Figure 1(i) shows another representative route to misfolding, with overdamped dynamics, and charges distributed along the edges. After buckling with same-signed curvature at the cusps, subsequent portions of the sheet join before the portion near the cusps has reached elastic equilibrium. These portions of the sheet have different-signed (upward) curvature, which persists in the final, nonclosed equilibrium shape (not shown).

Finally, we simulate the equator cut shown in Fig. 1(j). We have never been able to successfully fold this structure. Using quasistatic dynamics, the initial buckling at the cusps yields curvature of different signs, which persists in subse-

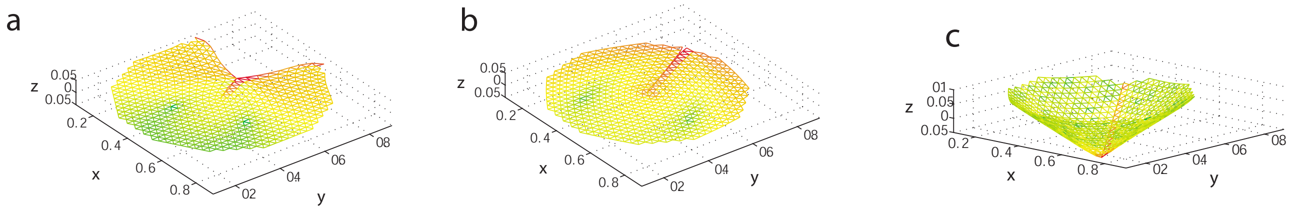

FIG. 2. (Color online) Sequences in the simulation of the assembly of a circular disk minus an angular sector into a cone by buckling. The parameter $\gamma = YR^2/\tilde{\kappa} = 625$ (where R is the total disk radius). The magnitude of stretching strain is visualized by intensity. Light gray (or green) corresponds to low values of strain and dark gray (or red) to high values. (a) The equilibrium disk shape with 1/3 of the edges zipped, with stretching strain insufficient to induce buckling. (b) The flat disk with edges completely zipped, prior to buckling. (c) The equilibrium conical shape of the zipped disk in (b).

quent states [Fig. 1(k)]. Different-signed curvature appears for an ensemble of random initial out-of-plane perturbations, and for all choices of orders in which different edges are joined. Also, different-signed curvature arises in all of our simulations using overdamped dynamics. In each case, a misfolded, nonclosed shape results.

The determining event for the correct assembly of the three shapes in Fig. 1 is the initial out-of-plane buckling at the cusps. At each cusp, buckling may occur with one of two signs. If the buckling events were independent, then a sheet with n cusps could buckle into 2^n possible configurations, only two of which can approximate a sphere (to the extent of having Gaussian curvature of a single sign). Therefore, successful assembly is generally favored by having a smaller number of cusps. Simulations show that coupling between cusps is important: using random perturbations to an initially flat sheet, the flower-petal cut tends to favor cusps buckling with the same sign of curvature, while the equator-cut sheet buckles with different-signed curvature. The latter prevents successful assembly. The rotational symmetry of the flower-petal sheet plays a role in correct assembly, since total stretching strain is reduced when all cusps buckle with the same sign of curvature.

The simulations also illustrate the contrast between assembly through local and global interactions. The strategy of joining edges is a local strategy which, as we have seen, leads to assembly through buckling. The strategy of joining the tips of the sheet, as in Fig. 1(e), is a global strategy, because the interaction of all six charges is important. Here electrostatic equilibria become important in addition to elastic equilibria, greatly increasing the number of equilibria and the possibility of misfolding. However, if the additional equilibria can be avoided, global assembly can succeed where the local zipping strategy does not. For the equator-cut shape, Boncheva *et al.* were able to obtain successful assembly using a dynamics in which first the equatorial loop closed, and then the poles. This is a global strategy, because it relies on first joining two edges with distance of the order of the sheet size to close the equatorial loop. This type of strategy puts constraints on the locations and strengths of the attracting elements, which must be considered as a fully coupled system.

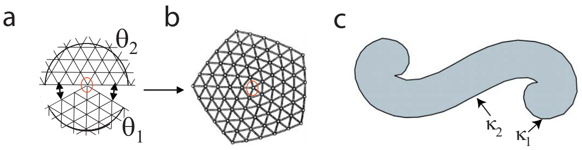

FIG. 3. (Color online) Diagram showing how dislocations arise in the joining of curved edges. (a) When two polygonal edges are joined near a a point (circled), a point disclination of strength $(\theta_1 + \theta_2) - 2\pi$ appears. The elastic equilibrium of the mesh is shown in (b). When two smooth edges are joined, the disclination density per unit length equals the sum of the curvatures κ_1, κ_2 of the joined points, as explained in the text (c).

III. ESTIMATION OF THE BUCKLING THRESHOLD

How do the shape of the cut and the sheet thickness affect buckling? The essential problem is captured by the buckling of a disk into a cone. In Fig. 2, a sector of angle $\pi/3$ has been removed from a disk, and attracting charges are placed on the resulting edges. When the sheet edges connect as in Fig. 2(b), large stretching energy is induced, with compression along radial lines and extension along circumferential lines. If the disk radius is sufficiently small, the disk remains planar. However, if the disk edges connect over a distance R which is sufficiently large, the sheet buckles out of plane. Here the stretching energy in the planar state is relieved by bending the sheet into a conical shape (with the curvature singularity cut off at the center), shown in Fig. 2(c).

A theoretical analysis of this buckling problem was given by Mitchell and Head [13] and subsequently by Seung and Nelson [11], who showed that the stretching energy in a flat disk of radius R with a sector of angle s removed grows as Ys^2R^2 for large R. The bending energy for the same sector bent into a developable cone, and cut off at inner radius a, grows only as $s\tilde{\kappa}\log(R/a)$, albeit with a larger prefactor. Hence, for fixed s, there is a critical radius above which the cone has lower energy than the disk. In nondimensional terms, this crossover radius R corresponds to a critical ratio of stretching to bending energy, or von Karman number,

$$\gamma = YR^2/\tilde{\kappa}. \tag{2}$$

For the disk in Fig. 2, the critical γ for buckling is $\gamma_{cr} = 154$ [11].

The buckling of a cone is a useful model to understand the buckling of more general shapes, such as the flower cut in Figs. 1(a)–1(d). Joining each of the six pairs of edges creates a local pattern of stretching strain similar to that in the disk. Here the particular shape of the joined edges determines the buckling threshold. For two curved edges meeting

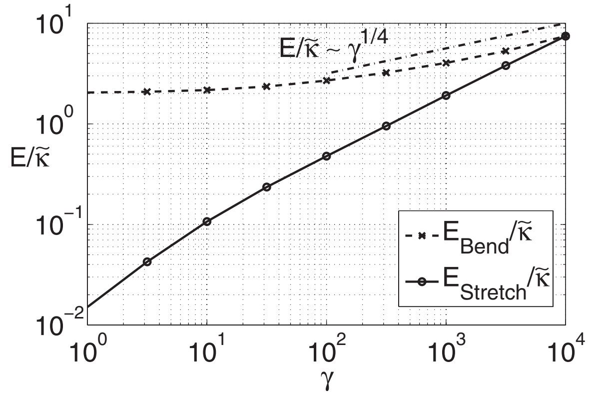

FIG. 4. Scaling of bending and stretching energies, nondimensionalized by $\tilde{\kappa}$, versus von Karman number γ, for the orange peel cut [Fig. 1(h)]. The bending energy increases from the value for an approximate sphere ($\gamma \ll 1$) concurrently with the appearance of a boundary layer for $\gamma \gg 1$. The predicted power-law scaling of $E/\tilde{\kappa}$ at large γ is shown for comparison up to $\gamma = 10^4$, when discretization effects become important. The stretching energy transitions from a linear growth ($E \sim \tilde{\kappa}\gamma$) to an intermediate scaling when subdominant to the bending energy for $10 < \gamma < 10^4$. The asymptotic calculation predicts that both energies scale as $\tilde{\kappa}\gamma^{1/4}$ for $\gamma > 10^4$.

at a cusp, we show now that the joined edges contain a line distribution of disclinations, with strength proportional to the difference between the curvatures of the two edges.

First, consider two edges of a sheet in our discretized model [Eq. (1)] which are forced together in a neighborhood of a point which is circled in Fig. 3(a). The two edges have interior angles $\theta_1 = 2\pi/3$ and $\theta_2 = \pi$ at this point. After the two edges are forced together, and the sheet is allowed to relax, for sufficiently small γ the sheet remains planar and the deformed configuration is shown in Fig. 3(b), with a stretching strain that is maximum at the circled point. The disclination strength is $(\theta_1 + \theta_2) - 2\pi$, which equals $-\pi/3$ in this case.

Now consider a sheet with a smooth boundary curve, shown in Fig. 3(c). Such a curve may be approximated by a polygonal curve that follows the edges of a hexagonal lattice. Each pair of points on the smooth boundary curve that are joined may be approximated by a pair of points on the polygonal curve that are joined in the manner shown in Fig. 3(a). Each pair of joined vertices contributes a disclination of strength $(\theta_1 - \pi) + (\theta_2 - \pi)$ over a lattice spacing ℓ. In the limit that ℓ tends to zero, the disclination strength per unit edge length equals

$$f(s) = \kappa_1(s) + \kappa_2(s), \tag{3}$$

the sum of the curvatures at the edges of the smooth curve.

When two curved edges are zipped together starting from a cusp, the radius at which buckling occurs corresponds to a critical value of γ. The sheet buckles when the edges are joined over a distance R_b that satisfies

$$\int_0^{R_b} f(s)ds = \phi > c12(1-\nu^2)(h/R_b)^2. \tag{4}$$

The inequality on the right was given by Seung and Nelson for a positive point disclination of strength ϕ in a circular disk of radius R_b, in which case c was estimated as 123 [11]. By including the new integral term on the left, we predict a similar inequality when ϕ is set equal to the disclination per unit length f integrated along the zipped edges. We use the same value of c as a first approximation, since it varies by less than for 20% for positive and negative point disclinations of the same magnitude [11]. In using the disk model of buckling at a cusp, we also assume that R_b is sufficiently small relative to the minimum distance between cusps so that each cusp buckles nearly independently.

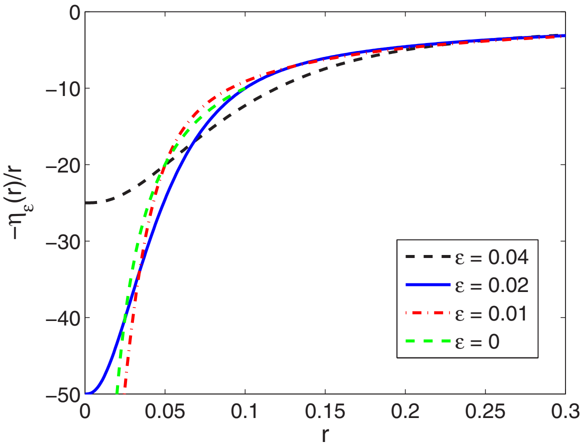

FIG. 5. (Color online) Charge potential with cutoff versus r.

We can express the term on the left-hand side of Eq. (4) more simply as

$$\int_0^{R_b} f(s)ds = \int_0^{R_b} \kappa_1(s) + \kappa_2(s)ds = [\theta]_{R_b,1}^{R_b,2}, \tag{5}$$

which is the change in tangent angle between the two points that are to be joined at a distance R_b from the cusp. In the experiment of Boncheva *et al.*, $h = 240\ \mu$m, while the edge lengths range from 20 mm (equator cut) to 80 mm (orange peel). Hence for all the edge pairs in the experiment the right-hand side of Eq. (4) is at most 0.189, while the left-hand side of Eq. (4) is at least $\pi/3$, so that buckling is predicted in all cases. By contrast, if the sheet were too thick, the edges too short, or the change in tangent angle too small—so that the inequality (4) were not satisfied—attraction between edges would be insufficient to induce buckling. In this regime assembly requires external forces.

IV. STRAIN CONCENTRATION IN BOUNDARY LAYERS AT EDGES

In addition to determining the occurrence of out-of-plane buckling of a sheet, dislocation-mediated stretching also determines the elastic energy in the final equilibrated state. The closed shapes in Fig. 1 show residual strain along the zipped edges. The energy E of these structures in the final state was examined in Boncheva *et al.* and estimated to be the bending energy of a sphere, $E \sim \tilde{\kappa}$. We find that this is correct only when the closed structure is exactly developable—in other words, it represents a locally area-preserving deformation of the flat sheet. However, this is a very special limit for zipped surfaces.

Generic regions do not form developable surfaces when zipped. In general, the shape of the sheet boundary plays an important role in the concentration of stress. The local shape of the two edges being zipped together acts as a source of stretching, leading to a localization of strain near the boundary. In Figs. 1(c) and 1(g) we show the flower-cut and orange peel shapes for $\gamma=10^4$ and 10^5, respectively, where the shading shows a stress concentration near the edges. Such concentrations have been examined for crumpled sheets where stress concentrates at points [14] and ridges [15]. There are typically large stretching and bending strains, which diverge within localized regions as the sheet thickness tends to zero. When stress is assumed to concentrate at an edge, an asymptotic calculation (Appendix B) predicts that elastic energies scale as $E \sim \tilde{\kappa}\gamma^{1/4}$. Figure 4 gives the stretching and bending energies versus the von Karman number $\gamma \sim (R/h)^2$ for the full numerical model of the orange peel cut discretized with 2200 faces. For $\gamma > 10^4$ the boundary layer thickness—the region of large stresses—is of the order of the bond length, so we are constrained to verify quantitatively the boundary-layer scaling over the range $10^2 < \gamma < 10^4$ where $\gamma \gg 1$. At $\gamma=10^4$, stretching and bending energy become equal, and we would expect both to increase as $\gamma^{1/4}$ for larger γ.

CONCLUSIONS

To conclude, our simulations have examined the relationship between sheet shape and self-assembly, and we have estimated how the number of metastable states depends on the shape of the sheet. Local minima increase exponentially with the number of edge pairs that exceed a sheet-thickness-dependent threshold of curvature variation. The analysis demonstrates that in general there is a limit to the complexity of an elastic sheet which can self-assemble without misfolding.

ACKNOWLEDGMENTS

The research reported in this paper was supported by the NSF-DMS (S.A.), as well as the NSF through Grant No. DMS-0296056 and the Harvard MRSEC.

APPENDIX A: ENERGY CUTOFF

A common method for simulating the dynamics of charged objects (such as molecules) is to introduce a cutoff ϵ so that the Coulombic potential is of the form $1/(r+\epsilon)$. In this case the gradient is large and discontinuous at $r=0$. We eliminate this discontinuity by removing the order-r term in the Taylor series expansion of the energy about $r=0$. Our energy is shown in Fig. 5 for several values of ϵ, in terms of the cutoff function

$$\eta_\epsilon(r_{ij}) = \frac{r_{ij}}{r_{ij}+\epsilon} + \frac{r_{ij}^2}{\epsilon^2}e^{-r_{ij}/\epsilon}, \tag{A1}$$

where ϵ is set to less than 10% of the equilibrium lattice spacing. For ϵ sufficiently small, the particular value of ϵ has a very small effect on assembly dynamics. For r on the order of the length between the nearest charges at each zipping step, the potential converges to the long-range $1/r$ electrostatic potential.

APPENDIX B: EDGE ENERGY CALCULATION

Here we give the calculation of the scaling of elastic energy with respect to material parameters for a shape formed by joining edges. Near a point $\mathbf{r}$ on the sheet edge, we may express the shape of the sheet in terms of the Foppl–von-Karman equations [17]:

$$\frac{Yh^3}{12(1-\nu^2)}\nabla^4 w = h[\phi, w], \tag{B1}$$

$$\nabla^4\phi = -\frac{Y}{2}[w,w] + F(\mathbf{r}), \tag{B2}$$

where

$$[a,b] = \frac{\partial^2 a}{\partial x^2}\frac{\partial^2 b}{\partial y^2} + \frac{\partial^2 a}{\partial y^2}\frac{\partial^2 b}{\partial x^2} - 2\frac{\partial^2 a}{\partial x\,\partial y}\frac{\partial^2 b}{\partial x\,\partial y}. \tag{B3}$$

Here w is the deflection out of the local tangent plane to the sheet edge (with rectilinear coordinates x and y), and ϕ is the Airy stress function [17]. These equations arise when taking the variation of the continuum elastic energies with respect to displacements, and using $\tilde{\kappa}=Yh^3/[12(1-\nu^2)]$. Here Y is the 3D Young's modulus, and ν is the Poisson ratio. We have included in Eqs. (B1) and (B2) a term $F(\mathbf{r})$ which represents a point source of in-plane stretching (such as a point disclination). For a point disclination, $F(\mathbf{r})$ is the product of disclination strength with a 2D δ-function. For a pair of curved zipped edges, corresponding to a continuous line of disclination density, $F(\mathbf{r})$ becomes the product of disclination density with a 1D δ function distribution across the boundary line. In Eq. (3) we gave the strength of the line distribution of disclinations as $[\kappa_1(s)+\kappa_2(s)]$. If we define a local coordinate frame with normal distance n and tangential distance s along the line, our source term becomes

$$F(\mathbf{r}) = \psi(s)[\kappa_1(s) + \kappa_2(s)]\delta(n). \tag{B4}$$

We have included a "rotation factor" $\psi(s)$ in this expression. If the boundary conditions require that the edges are clamped together—as is the case if the edges are joined by magnetic dipoles which apply a torque, as in the experiment of Boncheva *et al.*—then the two edges meet in the same tangent plane, and $\psi(s)=1$, representing purely in-plane stretching. If the edges are brought together by point charges, they are pinned together, in which case their relative position is fixed but they are free to rotate with respect to one another. In this case, some of the local stretching may be relieved by edge rotation, and generally $0 < \psi(s) < 1$. The form of ψ depends on the global 3D geometry of the sheet.

Returning to Eqs. (B1) and (B2), we insert Eq. (B4), and also change from rectilinear x,y coordinates to s,n coordinates. We now apply our assumption of a boundary-layer solution, so that all quantities vary more rapidly with n than with s. Thus we retain only the terms in Eqs. (B1) and (B2) with the largest number of n derivatives:

$$\frac{Yh^3}{12(1-\nu^2)}w_{nnnn} \approx \frac{h}{\rho}(w_{nn}\phi_n + w_n\phi_{nn}), \tag{B5}$$

$$\phi_{nnnn} + \frac{Y}{\rho}w_{nn}w_n \approx \psi(s)(\kappa_1 - \kappa_2)\delta(n). \tag{B6}$$

Here ρ is the radius of curvature of the (joined) boundary curve at point $\mathbf{r}$.

Following the argument by Lobkovsky and Witten [12], we nondimensionalize Eqs. (B6) by defining

$$\bar{\phi} = \phi/\tilde{\kappa}, \quad \bar{w} = w/\rho, \quad \bar{s} = s/\rho, \quad \bar{n} = n/\rho, \quad \bar{\delta} = \rho\delta, \tag{B7}$$

where we nondimensionalize lengths by the local radius of curvature of the boundary. For the quasidevelopable spheres considered here, ρ is of the order of the size of the assembled object. Upon inserting these expressions and dropping the overbars, the von Karman equations become

$$w_{nnnn} \approx (w_{nn}\phi_n + w_n\phi_{nn}), \tag{B8}$$

$$\lambda^2\phi_{nnnn} + w_{nn}w_n \approx \psi(s)(\kappa_1 - \kappa_2)\delta(n), \tag{B9}$$

where $\lambda = h/(12\rho\sqrt{1-\nu^2})$ is a nondimensional sheet thickness. We now assume that all the boundary-layer variables scale with different powers of sheet thickness:

$$\tilde{w} = \lambda^{\beta}w, \quad \tilde{\phi} = \lambda^{\epsilon}\phi, \quad \tilde{s} = s, \quad \tilde{n} = \lambda^{\beta}n, \quad \tilde{\delta} = \lambda^{-\beta}\delta. \tag{B10}$$

Here $\lambda^{-\beta}$ is the assumed width of the boundary layer; no rescaling is needed in the tangential s direction. We have also assumed that $\tilde{w}$ scales with $\tilde{n}$. This is because, as $\lambda \to 0$, the slope $d\tilde{w}/d\tilde{n}$ of the deformed plate undergoes an order-1 change across the boundary layer, the value of which depends on the global geometry of the closed surface. Finally, we have rescaled the δ function so that

$$\int \tilde{\delta}(\tilde{n})d\tilde{n} = \int \delta(n)dn = 1. \tag{B11}$$

We now determine the powers β and ϵ by balancing terms.

We insert the rescaled variables into Eqs. (B9) to obtain

$$\lambda^{3\beta}w_{nnnn} \approx \lambda^{2\beta-\epsilon}(w_{nn}\phi_n + w_n\phi_{nn}), \tag{B12}$$

$$\lambda^{2+4\beta-\epsilon}\phi_{nnnn} + \lambda^{\beta}w_{nn}w_n \approx \lambda^{\beta}\psi(s)(\kappa_1 + \kappa_2)\delta(n). \tag{B13}$$

A balance of terms in the two equations is possible only if $\beta = -\epsilon = -1/2$. Thus the boundary-layer thickness scales with the square root of the sheet thickness. This is the same scaling of the curved boundary layer that occurs in the mirror buckling of a sphere (or any convex surface) indented at a point [17,18]. The strength of the source term does not change the scaling of the curved boundary layer in a shell, but only the prefactor.

We can now determine how the elastic energy scales with sheet thickness. The stretching energy is given by

$$E_s = \frac{1}{2Yh}\int dx\, dy[\mathrm{tr}(\partial_i\partial_j\phi)]^2 - 2(1+\nu)\det(\partial_i\partial_j\phi). \tag{B14}$$

In the boundary layer the energy has the dominant term

$$E_s \sim \frac{1}{2Yh}\int dn\, ds \lambda^{1/2}\rho^2\left(\frac{\tilde{\kappa}\lambda^{-1/2}}{\rho^2\lambda^{1/2}}\right)^2\left(\frac{\partial^2\phi}{\partial n^2}\right)^2. \tag{B15}$$

Note that all quantities are rescaled by the corresponding powers of λ, although the tildes have been dropped for simplicity. Thus

$$\frac{E_s}{\tilde{\kappa}} \sim C\frac{\lambda^{-1/2}}{2}, \tag{B16}$$

where the constant C represents the evaluation of the integral. As for the mirror buckling of a sphere, we find that the stretching energy, nondimensionalized by the bending rigidity, scales as the sheet thickness to the $-1/2$ power. By similar steps, the same scaling holds for the bending energy (by necessity, since the two terms balance):

$$\frac{E_b}{\tilde{\kappa}} = \int dx\, dy[\mathrm{tr}(\partial_i\partial_j w)]^2 - 2(1-\nu)\det(\partial_i\partial_j w) \sim C'\frac{\lambda^{-1/2}}{2}. \tag{B17}$$

Since λ is a nondimensional sheet thickness, $\lambda \sim \gamma^{-1/2}$, so $E_s/\tilde{\kappa} \sim E_b/\tilde{\kappa} \sim \gamma^{1/4}$.

---

[1] M. Boncheva *et al.*, Proc. Natl. Acad. Sci. U.S.A. **102**, 3924 (2005).

[2] G. Whitesides and M. Boncheva, Proc. Natl. Acad. Sci. U.S.A. **99**, 4769 (2002).

[3] G. Whitesides and B. Grzybowski, Science **295**, 2418 (2002).

[4] M. Hoare and J. McInnes, Faraday Discuss. Chem. Soc. **61**, 12 (1976).

[5] P. Kralchevsky and N. Denkov, Curr. Opin. Colloid Interface Sci. **6**, 383 (2001).

[6] Y. Yin, Y. Lu, B. Gates, and Y. Xia, J. Am. Chem. Soc. **123**, 8718 (2001).

[7] I. Lee, H. Zheng, M. Rubner, and P. Hammond, Adv. Mater. (Weinheim, Ger.) **14**, 572 (2002).

[8] Y. Xia, Y. Yin, Y. Lu, and J. Mclellan, Adv. Funct. Mater. **13**, 907 (2003).

[9] B. Gates, Q. Xu, J. Love, D. Wolfe, and G. Whitesides, Annu. Rev. Mater. Res. **34**, 339 (2004).

[10] D. Wang and H. Mohwald, J. Mater. Chem. **14**, 459 (2004).

[11] H. Seung and D. Nelson, Phys. Rev. A **38**, 1005 (1988).

[12] A. Lobkovsky and T. Witten, Phys. Rev. E **55**, 1577 (1997).

[13] L. Mitchell and A. Head, J. Mech. Phys. Solids **9**, 131 (1961).

[14] E. Cerda and L. Mahadevan, Phys. Rev. Lett. **80**, 2358 (1998).

[15] A. Lobkovsky, Phys. Rev. E **53**, 3750 (1996).

[16] J. Nocedal and S. Wright, *Numerical Optimization* (Springer, Berlin, 2000).

[17] E. Landau and E. Lifshitz, *Theory of Elasticity* (Pergamon Press, Oxford, 1986).

[18] A. Pogorelov, *Bendings of Surfaces and Stability of Shells* (American Mathematical Society, Providence, RI, 1988).